

ENERGY BALANCE AT A COLD ALPINE FIRN SADDLE, SESERJOCH, MONTE ROSA

STEPHAN SUTER,^{a,*} MARTIN HOELZLE^{a,1} and ATSUMU OHMURA^b

^a *Versuchsanstalt für Wasserbau, Hydrologie und Glaziologie, Eidgenössische Technische Hochschule, CH-8092 Zürich, Switzerland*

^b *Institute for Atmospheric and Climate Science, Eidgenössische Technische Hochschule, Winterthurerstrasse 190, CH-8057 Zürich, Switzerland*

Received 23 May 2002

Revised 8 June 2004

Accepted 9 June 2004

ABSTRACT

Little knowledge exists to date on the complex interactions between the atmosphere and glaciers leading to the formation of cold firn in high-elevation accumulation areas in the Alps. Although the occurrence of cold firn and ice together is not a widespread phenomenon in the Alps, it is of particular significance as it relates to many glaciological issues, and has a major impact on glaciers in their role as an environmental and climatic archive. The atmospheric impact on cold firn was investigated using an energy balance study at the cold, 4300 m high firn saddle of Seserjoch, Monte Rosa area (Italy and Switzerland). Measurements of short- and longwave radiation, wind speed and wind direction, air temperature, humidity, snow height and snow and firn temperatures were conducted between September 1998 and August 2000 under difficult meteorological conditions. A 1 year time series of energy balance measurements spanning the period of May 1999 to April 2000 is presented. The results show that net radiation and turbulent heat fluxes are major elements of the energy balance. The heat fluxes due to surface melt in summer, and re-freezing events (re-freezing of meltwater at the surface, or rime accretion) cannot be neglected. The magnitude of these fluxes is difficult to interpret, as these are derived indirectly from the energy balance and, hence, also include instrumental and methodological errors in the energy balance calculation. Precise high-resolution measurements of surface temperatures in summer made it possible to identify individual surface melt events and the prevailing meteorological conditions favouring or hindering surface melt. Copyright © 2004 Royal Meteorological Society.

KEY WORDS: energy balance; cold glacier; surface temperature; melt energy; Alps; Monte Rosa

1. INTRODUCTION

The highest summit regions of the Alps are characterized by harsh climate conditions: nearly consistent sub-zero air temperatures, high rates of solid precipitation and high wind speeds. These conditions favour the formation of 'cold' firn and ice in the glacier accumulation areas, i.e. of firn and ice consistently maintaining temperatures below the freezing point. Such thermal conditions make glaciers a unique archive and an ideal venue for climate and environmental studies. A good understanding of the relevant energy- and mass-exchange processes at the atmosphere–snow boundary is crucial for understanding the processes that foster the formation of cold firn and for assessing possible thermal consequences for the englacial thermal regime in view of a potential climate change.

The near-surface thermal regime of cold firn and ice can only be fully understood by means of an energy balance study. Glacier melt in cold ablation areas is significantly reduced, resulting in lower degree-day factors (melt index according to the sum of positive degree days of air temperature) as the warming of cold

* Correspondence to: Stephan Suter, MeteoSwiss, Kräbühlstrasse 58, CH-8044 Zürich, Switzerland;

e-mail: Stephan.Suter@meteoswiss.ch

¹ Present address: Geographisches Institut Universität Zürich-Irchel, Winterthurerstrasse 190, CH-8057 Zürich, Switzerland.

ice represents a substantial heat sink (Konzelmann and Braithwaite, 1995). Basic aspects of the role of the energy balance and the single components in snow- and glacier-melt were, for example, considered by Kuhn (1987) and most recently by Ohmura (2001). The latter showed why air temperature can be taken as an influential proxy-parameter for glaciermelt.

Energy balance studies over snow extend back as far as the 1930s and 1940s (Sverdrup, 1936; Wilson, 1941). A series of modern energy balance (component-) measurements and modellings was carried out for Alpine glaciers (e.g. Föhn, 1973; La Casinière, 1974; Martin, 1975; Wagner, 1979, 1980; Escher-Vetter 1985a, b; Funk 1985; Oerlemans 1992, 2000; van de Waal *et al.*, 1992; Arnold *et al.*, 1996; Hock and Noetzli, 1997; Hock, 1999), mostly in connection with mass balance and glaciermelt–discharge investigations on temperate valley glaciers.

Physically based energy balance models, including all energy balance components, were successfully applied to complex Alpine topography to simulate spring snowmelt (Plüss, 1997; Fierz *et al.*, 1997), glaciermelt (Brock *et al.*, 2000), permafrost occurrence (Hoelzle *et al.*, 2001) and also avalanche forecasting (Brun *et al.*, 1989; Lehning *et al.*, 1999).

The objective of the present study is to investigate the energy and mass fluxes over a cold-firn surface, and to understand the conditions leading to the formation of cold firn.

2. FIELD OBSERVATIONS

2.1. Study area

Seserjoch, 4300 m a.s.l., is a cold glacier saddle situated at the heart of Monte Rosa, on the border between Italy and Switzerland (45°55'20"N, 7°52'00"E; Figure 1). The saddle is about 200 m in width and 300 m in length and has an ice depth of 103 m (O. Eisen, 2001, personal communication). The climate in the study area is characterized by high-altitude conditions, i.e. nearly consistent sub-zero air temperatures throughout the year, relatively high precipitation rates and high wind speed. Snow accumulation is strongly variable, ranging from 0.3 m water equivalent (w.e.) per year at wind-exposed saddles and ridges, to 2–3 m w.e. per year at wind-protected sites (Gäggeler *et al.*, 1983; Haeblerli *et al.*, 1983; Alean *et al.*, 1983; Eichler *et al.*, 2000).

The first meteorological investigations in the study area were carried out at Capanna Regina Margherita at the top of Signalkuppe, 4554 m a.s.l., in 1894, from 1927 to 1939, and from 1952 to 1958 during summer. Further meteorological observations were made at the end of the 1980s, with air temperature and snow height measurements at Colle Gnifetti from 1986 to 1990 (unpublished data from the Institute of Environmental Physics, University of Heidelberg), with meteorological observations at the saddle of Colle Vincent, 4087 m a.s.l., from 1991 to 1994 by the Italian Power Company ENEL and with the installation of a fully equipped weather station at Colle del Lys, 4250 m a.s.l. in 1996 by ENEL and the Università degli Studi di Milano (Rossi *et al.*, 2000a, b). A further very valuable data set for the area continues to be recorded at Gornergrat, 3135 m a.s.l., at the automatic weather station of the Swiss Meteorological Institute (MeteoSwiss) and the Swiss Federal Institute of Snow- and Avalanche Research (SFISAR) since 1993. The locations cited above are presented in Figure 1.

2.2. Instrumentation

The energy balance station was designed to measure the relevant heat fluxes over a snow surface. Two towers for the instruments of the energy balance measurements and two thermistor chains for measuring snow and firn temperatures (4 and 30 m total lengths) were installed at Seserjoch in September 1998 (Figure 2). Regular visits to the station for replacing, adding, repairing and maintaining the instruments were made at 1 to 4 month intervals. Most of the station was disassembled in August 2000. High-quality data were obtained between May 1999 and April 2000. Air temperature T and humidity H were measured at four levels above the surface, namely at 0.6 (level 4), 1.0 (level 3), 2.05 (level 2) and 3.1 m (level 1). Wind speed (WS) was measured at 1.0 (level 4), 1.4 (level 3), 2.5 (level 2) and 3.4 m (level 1). Additionally, shortwave radiation, longwave radiation, net radiation, surface temperature, wind direction and snow height were recorded by two

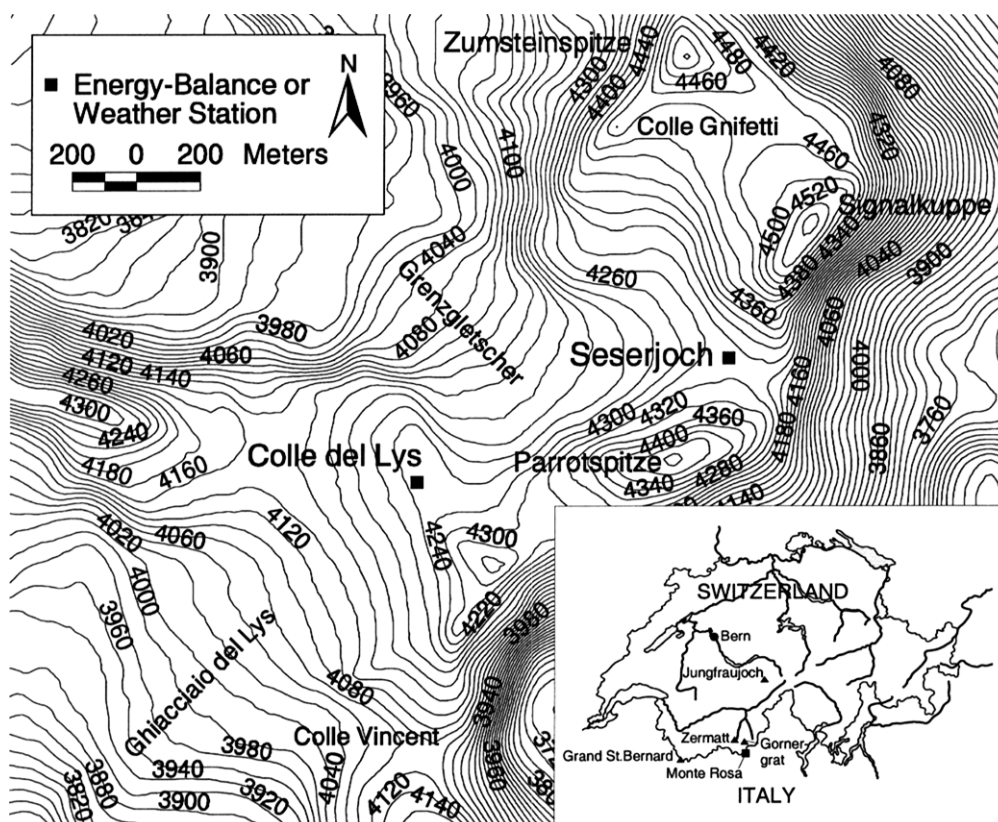


Figure 1. Overview of the study area of Sesejojoch, Monte Rosa showing the location of the energy balance station at Sesejojoch and of the weather station at Colle del Lys. The inset shows the location of the additional weather stations used in this study (triangles)

pyranometers (PM), two precision infrared radiometers (PIR), a net radiometer (NR), an infrared thermometer (IR), a potentiometer (WD) and a sonic ranging sensor (SH) respectively. Two thermistor chains (TS) of 4 and 30 m lengths were lowered into the glacier to measure the firn and ice temperatures at the site. The 4 m chain with 15 sensors at regular intervals of 0.25 m recorded the near-surface short-term temperature variations, whereas the 30 m chain, including 30 sensors at 1 m intervals, recorded the deep long-term temperature variations to an initial depth of 29 m. The characteristics of all sensors used are given in Tables I–III.

The data were stored on two separate data loggers: one for the firn temperature and the other for the climate data. Radio communications (ANT) to Zermatt and a telephone line to Zurich made it possible to retrieve data directly from the climate data logger and to control the instruments of the energy balance station remotely. The data-logging system, the additional electronics and the cabling were housed in a massive metallic box (CD). Power was supplied by up to three 36 Ah batteries (BAT) and up to two 50 W solar panels (SP). The instrumentation is shown in Figure 2.

The atmospheric data were recorded every 10 min, whereas the firn temperature measurements were stored every 30 min (4 m chain) and every 2 h (30 m chain). The main instrumental problems were caused by an occasional failure of the anemometers. The other instruments functioned with less trouble throughout the observation period.

2.3. Instruments and calibration

For the radiation measurements, a net radiometer, two pyranometers, two precision infrared radiometers and an infrared thermometer were used. The characteristics of the sensors are summarized in Table I.

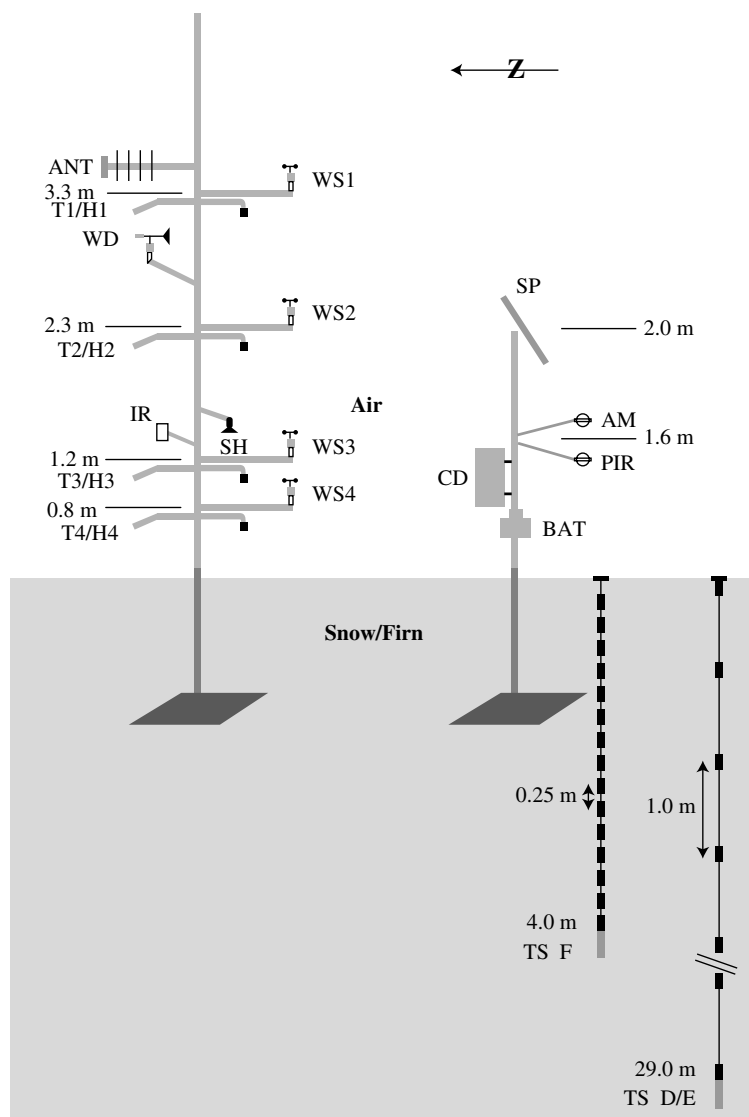


Figure 2. Instrumentation of the energy balance station at Seserjoch, Monte Rosa. See text for the abbreviations of the instruments. Initial instrument heights in May 1999 are shown

Table I. Characteristics of the radiation instruments. The range and the accuracy referred to are the technical specifications of the manufacturer

Instrument	Type	Quantity	Range	Resolution	Accuracy
Net radiometer	Swissteco S1	Net radiation	> 0.3 μm	0.06 W/m^2	better than $\pm 10\%$
Pyranometer	Kipp & Zonen CM 7B	Shortwave radiation	0.3–2.8 μm	0.25 W/m^2	$\pm 26 \text{ W}/\text{m}^2$ at 500 W/m^2
Precision infrared radiometer	Eppley PIR	Longwave radiation	3.5–50 μm	0.09 W/m^2	$\pm 6 \text{ W}/\text{m}^2$ at 200 W/m^2
Infrared thermometer	IRt/c.5	Surface temperature	–35 to 10 $^{\circ}\text{C}$	0.017 $^{\circ}\text{C}$	$\pm 1.5^{\circ}\text{C}$ at -10°C

The measurement range and the accuracy of the instruments are given in accordance with the technical specifications of the manufacturers.

The *resolution* of the sensor is usually determined by the sensitivity of the sensor under calibration conditions and by the measurement range and resolution of the data-logging system. The *accuracy* depends, on the one hand, on pure instrumental characteristics (e.g. resolution of the instrument, linearity of the signal, stability in time, azimuth dependency, temperature dependency, etc.) and, on the other hand, on ambient influences that are not directly linked with the instrument itself (e.g. atmospheric conditions, formation of surface dew or hoar on the instrument, etc.). Ambient effects are not included in the accuracy figures given in Table I.

The pyranometers and the infrared thermometer were recalibrated at the World Radiation Center (WRC), Davos, in September 2000 by comparing them with a corresponding reference instrument and by a calibration in a black-body cavity respectively. The sensitivities of the pyranometers determined by the initial calibration by the manufacturer and the calibration by the WRC accorded well. The WRC calibration was used for the transformation of the measured voltages to irradiances. Owing to technical problems during the calibration procedure, the calibration of the infrared thermometer performed by the WRC could not be applied. Instead, the initial calibration of the instrument performed by ALPUG (Alpine Umwelt und Gefahren) was applied. The voltages measured by the two precision infrared radiometers were transformed into irradiances using the calibration by the manufacturer. Corrections of the raw data were made in accordance with the recommendations by Philipona *et al.* (1995). No extra calibration was performed for the net radiometer and the calibration of the manufacturer used.

Table II presents the instruments that were used for the turbulence measurements and their characteristics. The sensors for air temperature were calibrated in a cold bath with circulation chiller of the type Huber CC245 with a 22 l internal bath and a warranted bath stability of $\pm 0.02^\circ\text{C}$. The bath temperature was controlled by four calibrated temperature sensors of the type Therm 2284-8. The system was calibrated at the Swiss Federal Office of Metrology in 1996. The absolute accuracy was certificated at $\pm 0.03^\circ\text{C}$ in the range between 0 and -10°C and at $\pm 0.04^\circ\text{C}$ between -12.5 and -20°C . The Pt-100 probes were calibrated with exactly the same instrumental setting as in the field at temperatures of -30 , -25 , -20 , -15 , -10 , -5 , 0 , $+5$ and $+10^\circ\text{C}$. Measurements were made for periods of typically half an hour after a good thermal adjustment of the sensors was achieved. The bath stability was in the range of ± 0.02 to $\pm 0.1^\circ\text{C}$, but normally at about $\pm 0.05^\circ\text{C}$. The relative accuracy of one and the same sensor can be denoted by $\pm 0.01^\circ\text{C}$ (see Table II), whereas the absolute accuracy can be denoted by $\pm 0.05^\circ\text{C}$. Measured (air) temperatures of a sensor were converted into calibrated temperatures using a linear interpolation between the calibration points of the individual sensor. No calibration was performed for the humidity sensors. A relative comparison between the sensors showed a good agreement (mean differences of only 0.02 to 0.12% were observed) during a pre-field comparison. The observed differences were taken into account for the data evaluation. No extra calibration was performed for the cup anemometers, the wind direction sensor or the sonic anemometer.

Table II. Characteristics of the instruments used for turbulent fluxes. The range and the accuracy referred to are the technical specifications of the manufacturer

Instrument	Type	Quantity	Range	Resolution	Accuracy
Temperature sensor	Vaisala HMP45DSP	Air temperature	-40 to 60°C	0.01°C	$\pm 0.2^\circ\text{C}$ at 20°C
Humidity sensor	Vaisala HMP45DSP	Relative humidity	0.8 – 100%	0.1%	$\pm 2\%$ at 0 – 90% $\pm 3\%$ at 90 – 100%
Cup anemometer	Aanderaa 2740	Wind speed	0 – 79 m/s	0.04 m/s	$\pm 2\%$
Wind direction sensor	Aanderaa 3590	Wind direction	0 – 360°	1.3°	Better than $\pm 5^\circ$
Sonic anemometer	Gill Solent 1012R2A	Wind velocity components u , v , w Speed of sound	0 – 60 m/s	0.01 m/s	$\pm 1\%$ at 0 – 30 m/s $\pm 0.5\%$ at 0 – 30 m/s of wind speed

Table III. Characteristics of the snow-height and the snow-temperature sensors. The range, the resolution and the accuracy referred to are the technical specifications of the manufacturer

Instrument	Type	Quantity	Range	Resolution	Accuracy
Sonic ranging sensor	Campbell SR50	Snow height	0.5–10 m	0.1 mm	±1 cm or 0.4% of distance to target
Thermistor chain	YSI 44006	Snow and firn temperature	–80 to 250 °C	1370 Ω/°C at 0 °C	±0.2 °C at 0 °C

The specifications of the other instruments used at the energy balance site are summarized in Table III. The sonic ranging sensor was very reliable and the given accuracy of the manufacturer sufficient for the purpose of snow height measurements. The temperature dependency of the speed of sound was taken into account. The thermistor chains were calibrated at temperatures of 0, –3.5, –6.7, –13.3 and –17.9 °C using a similar instrumental set-up as for the air temperature sensors. The accuracy of the calibration was strongly influenced by the stability of the cold bath, the resolution and accuracy of the data-logging unit, the characteristics of the thermistors and the cable, and the absolute accuracy of the temperature measuring device. The absolute accuracy of a thermistor measurement was ±0.03 °C at 0 to –10 °C and ±0.04 °C at –12.5 to –20 °C. The relative accuracy between the thermistors of an individual chain using the same measuring bridge was ±0.02 °C.

3. METHODOLOGY

3.1. The energy balance of cold firn areas

The energy balance at a cold snow/firn surface can be expressed as

$$R + H + LE + S + M = 0 \quad (1)$$

where R is net radiation, H is sensible heat flux, LE is latent heat flux (evaporation, condensation and sublimation), S is subsurface or ground heat flux and M is heat flux due to surface melt or re-freezing of meltwater and supercooled water droplets (rime accretion) on the surface. Signs are designated as positive when these fluxes are heat sources for the surface. In general, the net radiation R and the turbulent fluxes H and LE make a major contribution to the surface energy balance. At such a high altitude, the sensible heat flux is normally a heat sink. The subsurface heat flux S is strongly dependent on the temperature distribution in the firn, and generally small. At Seserjoch, surface melt occurs only on relatively rare occasions during summer daytime, but can be a rather important short-term energy sink. When looking at the energy balance over snow and firn, it must be borne in mind that the surface geometry and the surface properties are not stable over time. Strictly speaking, one has to deal with a free surface which constantly evolves in time due to accumulation and erosion processes. Thus, the surface properties of the snow cover (e.g. albedo, surface roughness, etc.) constantly change and influence the energy fluxes. The results of observed energy fluxes are presented in Section 4.

3.2. Radiation

The net radiation was calculated using the following measured quantities:

$$R = K \downarrow - K \uparrow + L \downarrow - L \uparrow \quad (2)$$

where $K \downarrow$ is the shortwave incoming radiation, $K \uparrow$ is the shortwave outgoing radiation, $L \downarrow$ is the longwave incoming radiation and $L \uparrow$ is the longwave outgoing radiation. The longwave outgoing radiation was

determined by both the PIR and the IR thermometer. The net radiometer was not used for determining the net radiation. It was strictly a back-up instrument. The data of the net radiometer were only used for May 1999, when the PIRs had not yet been mounted. The handling of the net radiometer in the field was difficult, and self-heating problems of net radiometers under conditions of high global radiation and a corresponding underestimation of the measured net radiation are reported by, for example, Ohmura and Gilgen (1993) and Konzelmann and Ohmura (1995).

3.3. Turbulent heat fluxes

Turbulent heat fluxes were calculated using the eddy correlation, profile and bulk methods. Although it is most common to use a 30 min averaging period for the calculation of the turbulent fluxes, in this study a time window of 10 min was adopted for three reasons:

1. The exposed firn saddle of Seserjoch is subject to major and rapid changes in the state of the atmosphere. Thus, the character of turbulence needs to be fully assessed by the time window selected as a compromise between a statistically stationary state of the atmosphere (which limits the averaging period) and the assessment of all high-frequency changes (which requires a certain minimum time window). The analysis of sonic data (see Section 4) showed that a 10 min time window was appropriate.
2. Since the sonic data were quite sparse and had data gaps, the use of 10 min values was the only way to achieve a reasonable analysis and comparison with the profile and bulk methods.
3. A 30 min resolution was too coarse for assessing high-frequency melt events during the day (see Section 4).

3.3.1. Profile method. As direct measurement of turbulent fluxes is a rather difficult task, this is often derived by measuring wind speed, temperature and humidity at different levels above the surface. The profile method or gradient–flux relationship assumes that the gradients of mean wind speed, mean (potential) air temperature and mean humidity are proportional to the corresponding shear stress, sensible and latent heat flux. The profile method is valid only in the atmospheric surface layer and over homogeneous surfaces. The gradient form of the wind profile and the non-dimensional gradients of temperature and humidity are written as

$$\frac{d\bar{u}}{dz} \frac{kz}{u_*} = \phi_m \left(\frac{z}{L} \right) \quad (3)$$

$$\frac{d\bar{\theta}}{dz} \frac{kz}{\theta_*} = \phi_h \left(\frac{z}{L} \right) \quad (4)$$

$$\frac{d\bar{q}}{dz} \frac{kz}{q_*} = \phi_q \left(\frac{z}{L} \right) \quad (5)$$

where \bar{u} is the mean horizontal wind speed, z is height above the surface, k is the von Kármán constant, u_* is a scaling parameter for wind speed (friction velocity), $\bar{\theta}$ is the mean potential temperature, θ_* is a scaling parameter for (potential) temperature, \bar{q} is the mean specific humidity, q_* is a scaling parameter for humidity and ϕ_m , ϕ_h and ϕ_q are non-dimensional stability functions of z/L , where L is the Obukhov length.

For the calculation of the wind and temperature profiles, the following relations were used (according to the number of useful levels):

$$x(z) = a \ln z + bz^2 + cz + d \quad (6)$$

or

$$x(z) = a + bz + c \ln z \quad (7)$$

where x is \bar{u} or $\bar{\theta}$, z is height above the surface and a , b , c , and d are coefficients. For the specific humidity profiles, the linear relation

$$\bar{q}(z) = az + b \quad (8)$$

was chosen. At high wind speeds, the wind profile at the Seserjoch firn saddle frequently showed a maximum wind speed at about 2.5 m height and a decreasing wind speed further above, possibly due to a jet effect. At low wind speeds, almost identical wind speeds at height could often be observed. The wind speed at the ground (at roughness length) was assumed to be zero. The lowest level of temperature measurements had to be omitted often, as it fit into the logarithmic profile form only in an inadequate manner. The measured surface temperature was taken at the height of the roughness length. The same can be stated for the lowest measurement level of humidity, which was also left aside in almost all cases. The other three levels often followed a good linear relation. Gradients of wind speed, potential temperature and specific humidity for a certain height above the surface were obtained as the derivative of Equations (6), (7) and (8). The stability functions $\phi_m(z/L)$, $\phi_h(z/L)$ and $\phi_q(z/L)$ were determined iteratively using the following relations for a gradient Richardson number $Ri > 0$ (Högström, 1988):

$$\phi_m = 1 + 6 \frac{z}{L} \quad (9)$$

and

$$\phi_h = \phi_q = 0.95 + 7.8 \frac{z}{L} \quad (10)$$

For an unstable stratification ($Ri < 0$), the following equations were used (Dyer, 1974):

$$\phi_m = \left(1 - 16 \frac{z}{L}\right)^{-0.25} \quad (11)$$

and

$$\phi_h = \phi_q = 0.74 \left(1 - 16 \frac{z}{L}\right)^{-0.5} \quad (12)$$

Cases under near-neutral conditions were eliminated by applying the following two selection criteria for excluding critical data from analysis (Högström, 1988):

- $u_* < 0.1$ m/s
- $|H| < 10$ W/m².

About 60% of the data had to be eliminated due to very small or negative values of u_* for the 1 year observation period.

The sensible heat flux H and latent heat flux LE were then calculated as

$$H = \rho_a c_p u_* \theta_* \quad (13)$$

$$LE = \rho_a L_v u_* q_* \quad (14)$$

where ρ_a is air density, c_p is specific heat of air at constant pressure and L_v is latent heat of vaporization.

3.3.2. Bulk method. The bulk method is an approximation of the turbulent heat fluxes from only one level of wind speed, temperature and humidity measurements. A constant gradient of these quantities is assumed between the level of measurement and the surface; therefore, surface values have to be assumed or measured. Surface temperature and humidity are well known for a snow surface when it is at melting conditions.

The surface temperature is 0°C and the vapour density is at saturation. For non-melting conditions, these quantities have to be measured or parameterized. When using the bulk approach, local gradients of wind speed, air temperature and humidity are replaced by corresponding finite differences between measurement level and surface. Based on these assumptions, a Bulk Richardson number

$$Ri_b = \frac{g \frac{\Delta \bar{T}}{\Delta z}}{\bar{T} \left(\frac{\Delta \bar{u}}{\Delta z} \right)^2} \quad (15)$$

can be defined, where g is acceleration due to gravity, \bar{T} is mean air temperature, z is height above the surface and \bar{u} is mean horizontal wind speed. The bulk Richardson number can be related to the stability functions for momentum (ϕ_m), heat (ϕ_h) and water vapour (ϕ_q) in the following way (Oke, 1987):

$$Ri_b \text{ positive (stable conditions)} : (\phi_m \phi_h \phi_q)^{-1} = (1 - 5Ri_b)^2 \quad (16)$$

$$Ri_b \text{ negative (unstable conditions)} : (\phi_m \phi_h \phi_q)^{-1} = (1 - 16Ri_b)^{0.75} \quad (17)$$

The turbulent fluxes for heat and water vapour are then calculated as follows (Oke, 1987):

$$H = \rho_a c_p k^2 z_u z_t \left(\frac{\Delta \bar{u} \Delta \bar{T}}{z^2} \right) (\phi_m \phi_h)^{-1} \quad (18)$$

$$LE = \rho_a L_v k^2 z_u z_q \left(\frac{\Delta \bar{u} \Delta \bar{q}}{z^2} \right) (\phi_m \phi_q)^{-1} \quad (19)$$

where $z_{u,t,q}$ are the log mean heights defined as

$$z_{u,t,q} = \frac{z - z_{0u,t,q}}{\ln \left(\frac{z}{z_{0u,t,q}} \right)} \quad (20)$$

The $z_{0u,t,q}$ denote the surface roughness lengths for wind, temperature and humidity. The roughness length is the height above the surface, where these quantities assume the surface value, and it is related to the general roughness of the surface.

Wind gradients were calculated using one wind-speed level (or the mean of two) in the air and the (assumed) zero wind speed at the surface roughness length for wind, which was determined as 0.001 m from the profile measurements. This is in good agreement with studies from, for example, Morris (1989) or Plüss (1997). For the sensible heat flux, the temperature gradient between one air temperature level (or the mean of two) and the measured surface temperature (taken from the PIR instrument or the IR thermometer) was used. Consequently, one level of measured relative humidity (or the mean of two) and an assumed surface humidity at saturation were applied to calculate the humidity gradient. Measured relative humidities were converted into specific humidities using

$$\bar{q} = 0.622 \frac{RHe_s}{p} \quad (21)$$

where \bar{q} is specific humidity, RH is measured relative humidity, e_s is saturation water-vapour pressure at a given air temperature and p is air pressure. The saturation water-vapour pressure was calculated using a formula by Lowe (1976). The specific humidity at the surface was calculated using the saturation water-vapour pressure for the observed surface temperature. A temperature-dependent latent heat coefficient was used to better consider the different thermal conditions of the surface.

3.3.3. *Eddy-correlation method.* The sensible heat flux H can be calculated directly from the eddy-flux relationship (e.g. Stull, 1988):

$$H = -\rho_a c_p \overline{w'T'} \quad (22)$$

where ρ_a is air density, c_p is specific heat of air at constant pressure, w' is deviation from the mean vertical wind velocity ($w' = w - \bar{w}$) and T' is deviation from the mean air temperature ($T' = T - \bar{T}$).

3.4. Subsurface or ground heat flux

The subsurface heat flux S was determined using

$$S = -K_i \frac{\Delta T}{\Delta z} \quad (23)$$

where K_i is the thermal conductivity of snow or firn, $\Delta T = T_s - T_z$, T_s is the surface temperature at depth $z_0 = 0$, T_z is the snow temperature at depth z_1 measured by the uppermost thermistor of the 4 m thermistor chain and $\Delta z = z_1 - z_0$. The thermal conductivity K_i is strongly dependent on the snow and firn density. It is found between 0.04 for very light snow and 2.21 W/(m K) for ice at 0°C. Although the near-subsurface temperature gradient can be quite high due to radiative cooling at night, it will seldom exceed 20°C/m. This would lead to a subsurface heat flux of approximately 20 W/m² for firn.

The thermal conductivity K_i was calculated as a mean between (1) the Schwerdtfeger formula (Paterson, 1994)

$$K_i = 2.1 \times 10^{-2} + 4.2 \times 10^{-4} \rho + 2.2 \times 10^{-9} \rho^3 \quad (24)$$

and (2) the van Dusen formula (Paterson, 1994)

$$K_i = \frac{2 K_{\text{ice}} \rho}{3 \rho_{\text{ice}} - \rho} \quad (25)$$

where ρ is the observed snow or firn density, K_{ice} is the heat conductivity of ice (2.1 W/(m K)) and ρ_{ice} is the density of ice (900 kg/m³). The Schwerdtfeger formula represents an upper limit and the van Dusen formula a lower limit. The observed density was assumed as a mean between a typical fresh snow value (250 kg/m³) and a higher value (500 kg/m³), which is typical for wind-packed or long-exposed snow. A thermal conductivity of 0.5 W/(m K) results. This value is not very sensitive; varying the density from 200 to 500 kg/m³ changes K_i from 0.2 to 0.7 W/(m K) only.

Snow and ice both allow some transmittance of radiation, which means that the incident radiation at the surface can be transmitted, reflected or absorbed in the snow cover. Reflection and absorption of radiation are largest in the uppermost centimetres of the snow cover. Absorption can lead to an important warming in the immediate surface layer. This warming is normally compensated by the longwave outgoing radiation at the surface. Ohmura (1984) investigated the transmission of net radiation on the lower side of a dry seasonal snow cover. He found the transmission of net radiation on the lower side of the snow cover to be in the order of the conductive heat flux at the bottom of the snow cover, and to be one order of magnitude larger than the conductive heat flux at the top of the snow cover for the period of 3 May to 6 June.

3.5. Melt and re-freezing

At the surface, the energy consumed by surface melt or released by re-freezing of liquid water can be written as

$$M = L_f m_w \quad (26)$$

where L_f is the latent heat of fusion and m_w is the mass flux of water to be melted or re-frozen per unit area. The mass flux is negative during a melt event (mass loss at the surface due to percolation of meltwater) and positive during a re-freezing event. On a daily time scale, M can only be negative if there is a discharge of meltwater at the surface. Otherwise, the meltwater will re-freeze *in situ* and M will be approximately zero. Freezing of liquid water at the surface can occur by re-freezing of meltwater or by ad-freezing of supercooled water droplets in clouds or fog (hoar frost or rime accretion). Surface melt at the Seserjoch site is limited to a few events during summer. An individual event can turn over quite an important amount of energy on a daily time scale. On a longer time scale, the absolute energy input to the snow- and firn-cover due to frequent melt events with corresponding re-freezing of meltwater in deeper snow and firn layers can be important and have a major influence on the prevailing mean firn temperature (Suter, 2002). Especially at sites with a high radiation income and/or generally low wind speeds, melt-layer formation becomes frequent and can change the temperature regime of the snow and firn considerably (Beck *et al.*, 1988).

The practical problem in calculating the heat flux due to melt or re-freezing according to Equation (26) lies in the determination of the mass flux which is melted or re-frozen. It is true that in a conventional mass balance investigation, ice layers from one melt season can be mapped in a snow profile. An assessment of the total melt energy from a melt season based on melt-layer analysis is difficult, however, as the formation of ice layers can be very heterogeneous in space. No daily resolution of the melt energy is possible. Although techniques exist to determine the free water content in a snow cover with a high temporal resolution, a continuous measurement is extremely difficult and delicate, as part of the meltwater re-freezes within a very short vertical distance, and because of the heterogeneous movement of the meltwater in the snow. The application of a simplified approach using, for example, a degree-day factor as a measure of surface melt according to the air-temperature degree-day sum (e.g. Braithwaite, 1992) is not suitable for the Seserjoch site either, as the maximum daily values exceeded the melting point only on rare occasions (about 12 events from July to September), and the observed daily mean air temperatures never did. Theoretical considerations (Kuhn, 1987) and laboratory experiments (Beck *et al.*, 1988) showed that surface melt events for cold snow and firn can also occur at negative air temperatures. Higher net radiation and air temperatures favour ice-layer formation, whereas high wind speeds and low air humidities have an inhibitory influence.

4. RESULTS FROM THE FIELD OBSERVATIONS

4.1. Air temperature

Figure 3 gives the monthly mean air temperatures for the period from May 1999 to April 2000. The mean air temperature for the observation period (or mean annual air temperature) is -11.2°C , as measured at the uppermost and most undisturbed level. A comparison with air temperature records (monthly mean values) from surrounding meteorological stations (see Figure 1 for locations) shows that the high-elevation sites of Jungfrauoch (3580 m a.s.l.) and Gornergrat (3135 m a.s.l.) have a very constant offset (Figure 3), resulting in an air temperature lapse rates of $-0.59^\circ\text{C}/100\text{ m}$ (Jungfrauoch) and of $-0.68^\circ\text{C}/100\text{ m}$ (Gornergrat). The higher lapse rate in the case of Gornergrat might point to drier and more continental conditions in the Monte Rosa area compared with the Jungfrau area. The offsets from the stations situated at lower elevations, i.e. Grand St Bernard (2478 m a.s.l.) and Zermatt (1638 m a.s.l.), are not as constant. In the case of the valley station of Zermatt, this is probably due to frequent temperature inversions during winter; in the case of Grand St Bernard, there might be synoptic reasons as well.

4.2. Snow accumulation and ablation

Figure 4 shows the evolution of the daily accumulation and ablation measured by the Campbell SR50 sonic ranging sensor at Seserjoch from May 1999 to April 2000, referring to the level at the start of the measurements in September 1998. The pattern shows that the main accumulation occurs from about April to November, whereas practically no accumulation can be observed in high winter due to very low temperatures, prevailing dry conditions and wind erosion.

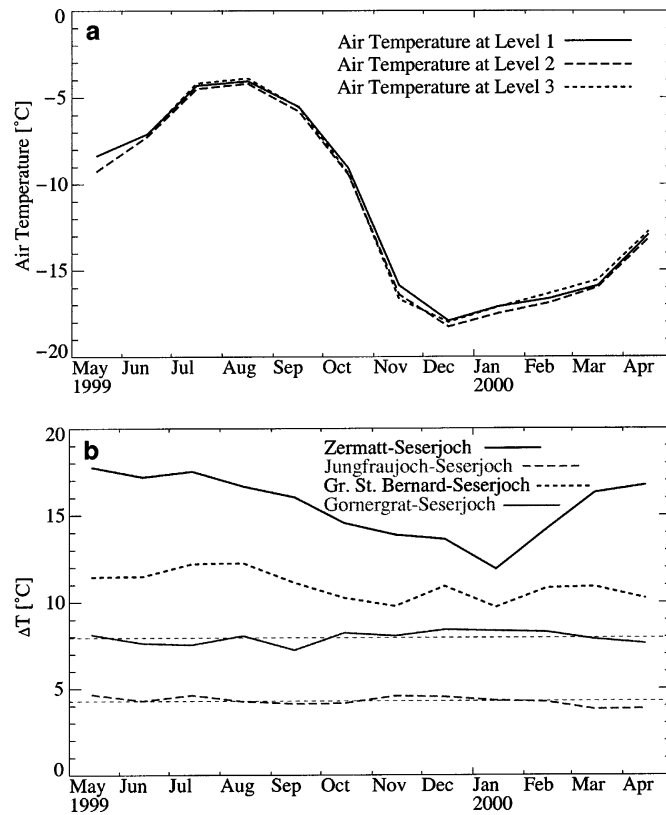


Figure 3. Air temperature (monthly mean values) at Sesarjoch (Monte Rosa) from May 1999 to April 2000 (a) and offset to surrounding meteorological stations (b). The mean offsets (May 1999 to April 2000) to the Jungfrau-Sesarjoch and Gornergrat air temperatures are given with thin dashed lines. See Figure 1 for locations of weather stations

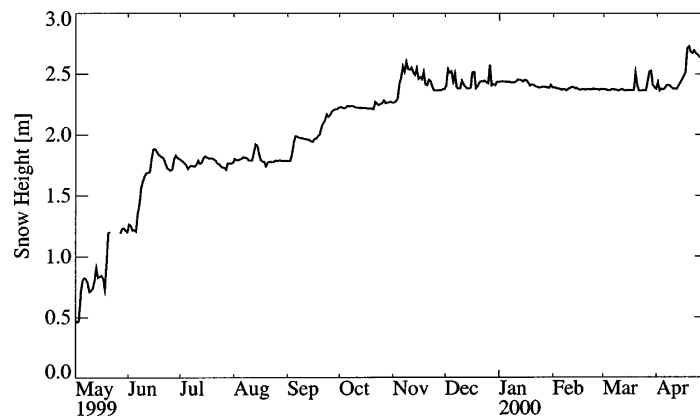


Figure 4. Accumulation and ablation (daily mean values) at Sesarjoch (Monte Rosa) from May 1999 to April 2000. The zero reference level is taken to be the level at the start of the measurements in September 1998

4.2. Radiation and surface temperature

The monthly mean values of net radiation are presented in Figure 5. The deviations between the calculated net radiation using the PIR instrument or the IR thermometer are minor and typically in the order of 3 to 9 W/m². The calculated net radiation using the outgoing radiation of the IR thermometer gives higher values

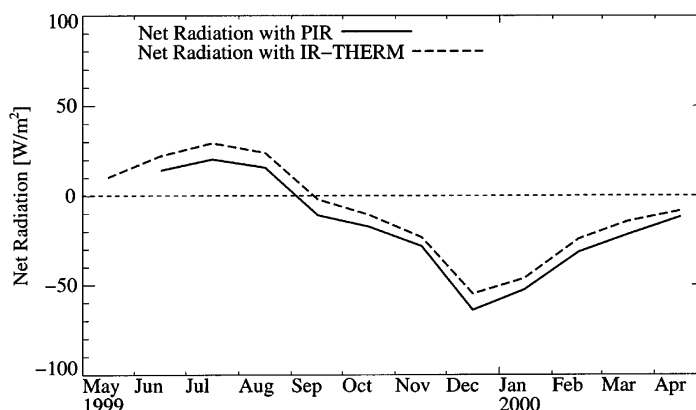


Figure 5. Net radiation (monthly mean values) at Sesarjoch (Monte Rosa) from May 1999 to April 2000. The net radiation measured by the net radiometer is shown for May 1999

due to a reduced amount of outgoing radiation by the IR thermometer. As one would expect, the net radiation is positive during the months with high shortwave incoming radiation (May to August) and negative during the 'winter' months (September to April).

The effective surface temperature by the IR thermometer was, on average, 2 °C deeper on the monthly scale (Figure 6). The generally deeper values for the surface temperatures observed with the IR thermometer can be explained by the use of an instrument temperature that was too low, as the instrument temperature of the (unventilated) IR thermometer had to be replaced by a (ventilated) air temperature and by a smaller absolute accuracy of the IR thermometer in general.

4.4. Turbulent heat fluxes

4.4.1. Eddy-correlation method. From 26 to 29 May 1999, eddy correlation measurements were carried out at Sesarjoch using a three-dimensional sonic anemometer of the Gill Solent 1012R2A type at a sample frequency of 21 Hz (see Table II). The instrument was mounted 2.1 m above surface.

The measured sensible heat flux showed a typical diurnal pattern for the observation period with negative values during daytime and positive values after sunset, when the negative radiation balance was compensated. The magnitude of the flux was rather small and never exceeded 30 W/m². Although the *footprint* of the sonic anemometer (distance sensed by the instrument) was in the order of 5–10 m only, the instrument height of

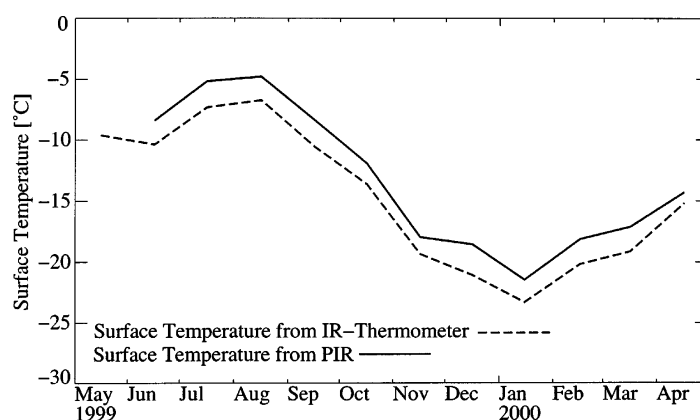


Figure 6. Surface temperatures (monthly mean values) at Sesarjoch (Monte Rosa) from May 1999 to April 2000 measured with the IR thermometer and derived from the measured longwave radiation by the PIR

2.1 m was presumably still too high. Strong horizontal air advection in this layer probably made it impossible to see the small-scale eddies below the instrument. Further investigations using an array of sonic anemometers at different levels above the surface and in space would be necessary to make a statement on the character of turbulence at the site.

4.4.2. Comparison with indirect methods. The two indirect methods (profile and bulk) showed a smaller sensible heat flux at 2.1 m from 27 to 29 May 1999 than the one determined by the sonic anemometer. This means that either the sensible heat flux measured by the sonic anemometer is representative only for the height in question, but not for the actual turbulent exchange at the surface, or that the profile and bulk methods considerably overestimate the fluxes. Owing to the stratification of the surface boundary layer at the time of observation, however, the first may be valid. Thus, a comparison between the sonic anemometer and the other methods is difficult. Nevertheless, a certain confidence in the flux calculations is generated by the fact that (in the absence of melt) the turbulent fluxes have to adopt a certain magnitude to compensate the radiative flux on a daily time scale, and by the fact that the signs of the fluxes coincide in the majority of cases.

In Figure 7 the daily mean values of sensible and latent heat flux from May 1999 to April 2000 are compared using the profile and bulk methods. Flux directions are mostly correct, but there can still be large scattering between single observations.

4.5. Subsurface or ground heat flux

The subsurface heat flux over snow or firn is normally small (Figure 8) due to the fact that the surface temperature cannot rise above 0°C. The maximum daily value found is about 5 W/m². As the temperature gradient is mainly negative from May to September (colder snow temperature than surface temperature), predominately negative fluxes can be observed in this period. From October to mid-April, the opposite is the case. Even if one assumes that short-term temperature gradients of 20°C/m occur, the subsurface heat flux would not exceed 10 W/m².

The heat flux due to transmitted net radiation was found to be in the order of the conductive heat flux at the top of the snow cover. Since the uppermost thermistor of the 4 m chain was increasingly buried under snow later on, the heat flux due to transmission of net radiation was not considered for the energy balance series from May 1999 to April 2000.

4.6. Melt and re-freezing

Melt events at the Seserjoch site could clearly be identified by the measured surface temperatures, which quite frequently showed 0°C during the day in July and August (Figure 9) and on few occasions in September.

Although the occurrence and duration of melt events can clearly be identified (see Table IV; Figure 9), the mass turnover cannot be determined, nor can the heat flux due to melt (or re-freezing) be directly calculated. The determination of the energy balance, however, allows an estimate of these fluxes when looking at the residual heat flux, which (besides the inherent errors) contains the energy flux due to melt and re-freezing. A good correlation between the measured surface temperatures and the calculated daily mean residual heat flux can be found, for example for August 1999 (Figure 9). During melt events, the residual heat flux is predominately negative, indicating an energy surplus that is compensated by melt. During the phases with no melt, re-freezing processes (e.g. rime accretion) can occur.

Figure 10 shows two examples for melt and re-freezing from 4 and 16 August. Although air temperature is below the freezing point in both cases, melt does occur in the first case due to a high net radiation and relatively low wind speeds. In the latter case, net radiation is much smaller and wind speed is high, which inhibits melt. Both air humidities are high. The quite large residual energy flux at night may be due to re-freezing processes (either re-freezing meltwater or rime accretion due to fog).

As surface melt events are crucial for the thermal regime of the firn, Table IV summarizes the results from the 1999 melt season at Seserjoch giving the number of melt days, the duration of melt and the melt-energy input as monthly (mean) values or yearly totals. The values were calculated using the 10 min values of IR

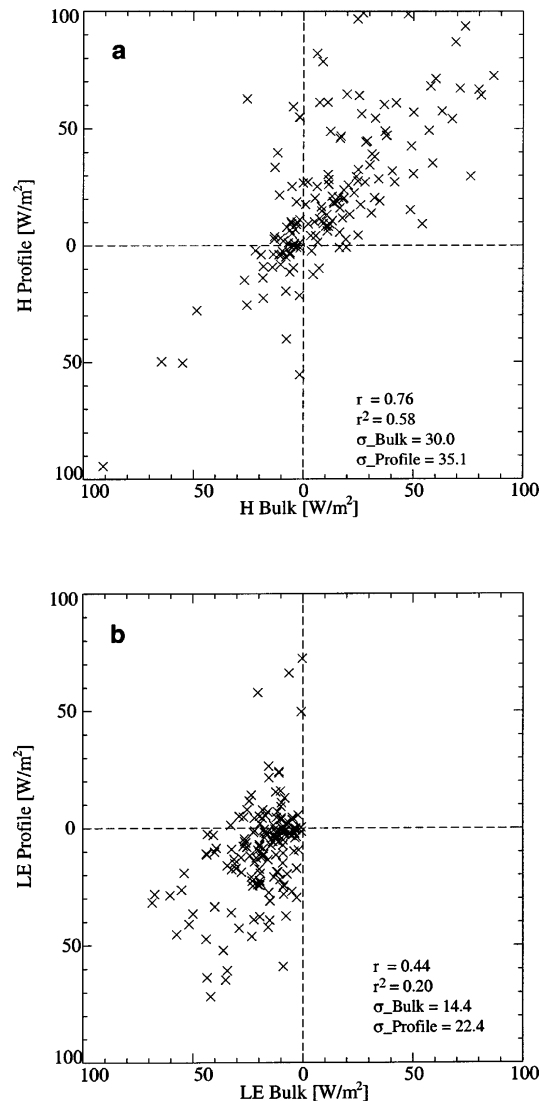


Figure 7. Comparison of daily mean values of sensible (a) and latent (b) heat flux using the bulk and profile methods from May 1999 to April 2000

thermometer or PIR surface temperatures and the negative residual heat flux derived from the energy balance calculation. Calculations were made for assumed melting conditions at surface temperatures T_s greater than -1.0 or -0.5°C or equal 0°C to account for the accuracy of the IR thermometer with $\pm 0.5^\circ\text{C}$ at 0°C and of the PIR with (estimated) values of $\pm 5 \text{ W/m}^2$ or $\pm 1.1^\circ\text{C}$ at 0°C .

4.7. The energy balance and the residual heat flux

Monthly mean values of the energy balance using bulk and profile methods are presented in Table V and Figure 11. The *residual heat flux* comprises the melt flux M and the instrumental and methodological errors of the net radiation, sensible, latent and ground heat flux. Owing to missing daily mean values, data gaps occur for the profile method.

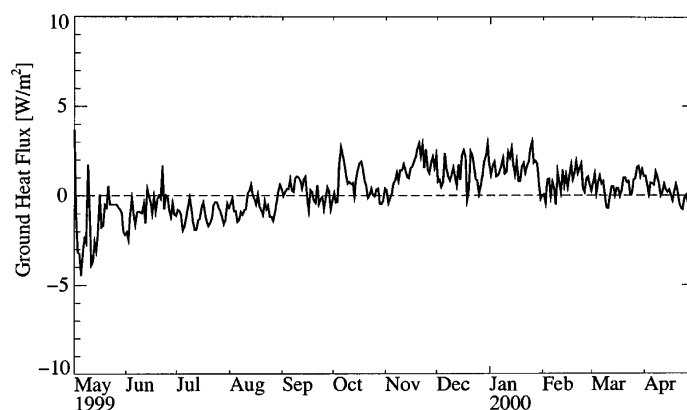


Figure 8. Subsurface heat flux at Seserjoch from May 1999 to April 2000

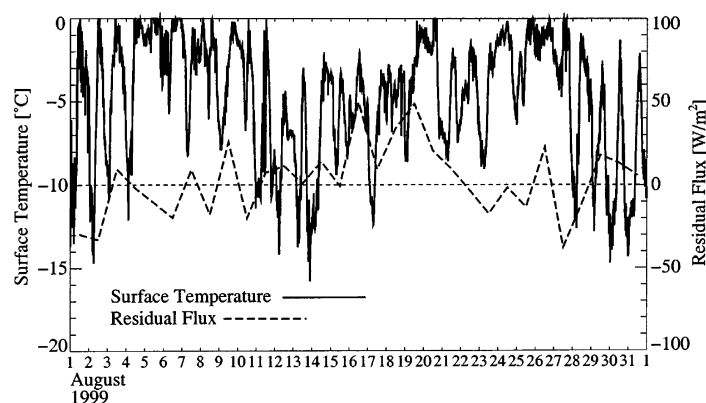


Figure 9. Surface temperatures and daily residual heat flux from August 1999 showing melt events at Seserjoch

Table IV. Summary of the monthly and yearly sum of melt days, the monthly mean and yearly total melt duration and the monthly mean and yearly total melt energy input at Seserjoch. Melt was assumed for surface temperatures T_s greater than -1.0 or -0.5 °C or equal to 0 °C

Time	Number of melt days			Mean daily melt duration (h)			Mean daily melt energy input (J/m^2)		
	0 °C	-0.5 °C	-1.0 °C	0 °C	-0.5 °C	-1.0 °C	0 °C	-0.5 °C	-1.0 °C
May 1999	4	4	5	0.47	0.58	0.70	0.00	0.02	0.05
Jun 1999	0	1	4	0.00	0.01	0.06	0.00	0.01	0.05
Jul 1999	18	21	22	0.99	1.83	2.95	3.91	6.11	8.60
Aug 1999	11	17	18	0.57	1.60	3.34	1.09	2.44	4.03
Sep 1999	3	4	5	0.06	0.12	0.21	0.19	0.31	0.50
Yearly total	36	47	53	65	128	225	13.88×10^6	23.78×10^6	35.39×10^6

A positive net radiation can only be observed from May to August. A quite large negative radiation balance occurs in December and January due to the lower solar elevation and the shading from the adjacent Parrotspitze (Figure 1), as well as very low longwave incoming radiation.

The monthly means of the ground heat flux are very small and play an unimportant role in the energy balance.

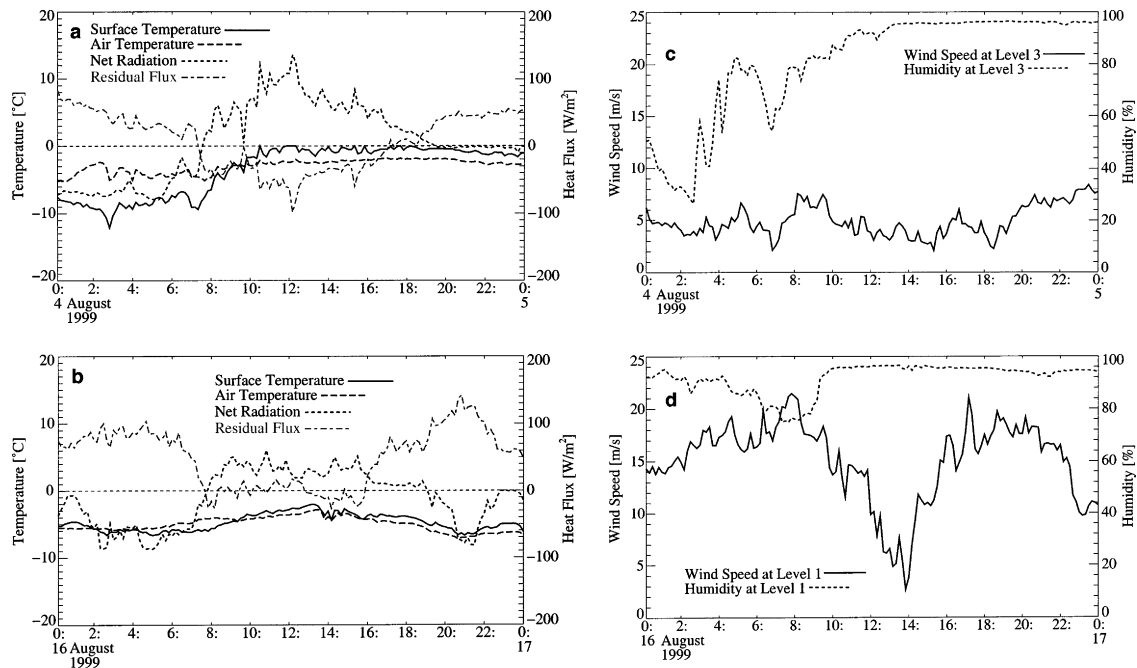


Figure 10. Surface and air temperatures, net radiation and residual heat flux from 4 August (a) and 16 August 1999 (b) and observed wind speeds and relative humidities from 4 August (c) and 16 August (d)

Table V. Summary of the monthly and yearly mean energy fluxes at Seserjoch showing the net radiation (NR), sensible heat flux (SHF), latent heat flux (LHF), ground heat flux (GHF) and the residual heat flux (RES). The turbulent fluxes are derived using the bulk and the profile methods. The fluxes are given in W/m^2

Time	NR	SHF		LHF		GHF	RES	
		Bulk	Profile	Bulk	Profile		Bulk	Profile
May 1999	10.4	6.3		-6.5		-1.4	-8.8	
Jun 1999	14.3	11.6	29.0	-18.8	-9.9	-0.7	-6.4	-32.8
Jul 1999	20.4	5.2	28.3	-16.2	3.9	-1.1	-8.4	-51.6
Aug 1999	15.9	5.7	13.8	-24.1	-6.0	-0.5	3.0	-23.2
Sep 1999	-10.8	11.8		-12.2		0.2	10.9	
Oct 1999	-17.2	10.8		-7.7		0.7	13.4	
Nov 1999	-28.1	11.0		-10.6		1.5	26.2	
Dec 1999	-55.6	10.9		-20.7		1.3	64.0	
Jan 2000	-52.7	25.6		-10.0		1.5	35.6	
Feb 2000	-31.5	29.7	27.0	-17.6	-17.5	0.8	18.6	21.2
Mar 2000	-21.7	23.4	19.5	-18.5	-14.9	0.6	16.1	16.5
Apr 2000	-11.7	20.0		-20.4		0.2	11.2	
Mean	-14.0	14.3		-15.3		0.3	14.7	

The turbulent fluxes given by the bulk method show steady positive values for the sensible heat flux and negative values for the latent heat flux. Thus, the positive net radiation during the summer months is mainly compensated for by the latent heat flux; likewise, the negative net radiation in the winter months is compensated by the sensible heat flux. The negative residual heat flux during summer may be due to melt events. The residual heat flux from November to January is very high and must be explained by an

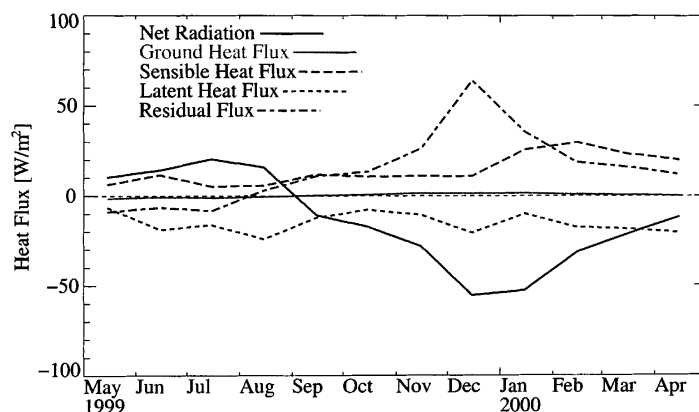


Figure 11. Monthly mean energy balance of May 1999 to April 2000 at Seserjoch using the bulk method

underestimation of the sensible heat flux, possibly due to an underestimation of the wind speeds caused by hoar frost at the instruments. Another part of the residual heat flux must be attributed to rime accretion at the surface. The generally rather high latent heat fluxes could be due to the assumption of water-vapour saturation at the surface.

The useful data calculated with the profile method are sparse. In the direction of the flux, they depict the conditions as calculated with the bulk method, but the magnitude of the sensible heat flux is higher in summer.

5. CONCLUSIONS

This paper describes in full detail the energy balance of a cold glacier accumulation area in the Alps and the inherent difficulties and problems.

Although major contributions to the energy balance come from the net radiation and the turbulent fluxes, there is strong evidence that heat fluxes based on melt and re-freezing processes at the surface make an important contribution which cannot be neglected.

During the summer months (May–August) the positive net radiation is mainly compensated for by the negative latent heat and melt. In winter (September–April) the negative net radiation is predominantly equalized by the positive sensible heat and re-freezing at the surface (rime accretion).

The net radiation (high year-round albedo, low longwave incoming radiation) and the latent heat (predominantly evaporation and sublimation) are the most important energy sinks.

Generally, the turbulent heat fluxes were difficult to determine because of the application of turbulence theory under non-ideal conditions and instrumental problems due to severe weather situations. Under these conditions, the bulk method proved to be the most reliable method and assured continuous flux calculations.

The continuous observation of surface-melt events at a high resolution made it possible to quantify the energy input into cold firn during the melt season based on an energy balance approach.

We believe that the calculated energy input is within a very realistic order of magnitude, since the evolution of the firn temperature profile at the Seserjoch could accurately be reproduced for the observation period using the observed surface temperatures and melt energy input (Suter, 2002).

ACKNOWLEDGEMENTS

This research was supported by the European Union Environment and Climate Programme under ENV4-CT97-0639 and the Swiss Government under BBW Nr. 97.0349-1 within the framework of the ALPCLIM EU project (Environmental and climate records from high-elevation Alpine glaciers).

We gratefully acknowledge the valuable assistance of many students and colleagues at the Section of Glaciology of the Laboratory of Hydraulics, Hydrology and Glaciology (VAW) at ETH Zurich, the Institute

of Geography at the University of Zurich and the Institute for Atmospheric and Climate Science at ETH Zurich, in the strenuous field work in high-altitude conditions and in data analysis and interpretation. We are especially indebted to MeteoSwiss, Zurich (CH), Giancarlo Rossi, Noale (I) and to Rolf Philipona, World Radiation Center, Davos (CH), for providing data from surrounding meteorological and climate stations.

REFERENCES

- Alean J, Haeberli W, Schädler B. 1983. Snow accumulation, firn temperature and solar radiation in the area of the Colle Gnifetti core drilling site (Monte Rosa, Swiss Alps): distribution patterns and interrelationships. *Zeitschrift für Gletscherkunde und Glazialgeologie* **19**(2): 131–147.
- Arnold NS, Willis IC, Sharp MJ, Richards KS, Lawson WJ. 1996. A distributed surface energy-balance model for a small valley glacier. I. Development and testing for Haut Glacier d'Arolla, Valais, Switzerland. *Journal of Glaciology* **42**(140): 77–89.
- Beck N, Wagenbach D, Münnich K. 1988. Laboratory experiments on the formation of solar radiation induced melt layers in dry snow. *Zeitschrift für Gletscherkunde und Glazialgeologie* **24**(1): 31–40.
- Braithwaite R. 1992. Degree-day factor, energy balance, and the increased melting of the Greenland ice sheet under a warmer climate. *Rapport Grønlands Geologiske Undersøgelse* **155**: 79–83.
- Brock B, Willis I, Sharp M, Arnold N. 2000. Modelling seasonal and spatial variations in the surface energy balance of Haut Glacier d'Arolla, Switzerland. *Annals of Glaciology* **31**: 53–62.
- Brun E, Martin E, Simon V, Gendre C, Coleou C. 1989. An energy and mass model of snow cover suitable for operational avalanche forecasting. *Journal of Glaciology* **35**(121): 333–342.
- Dyer A. 1974. A review of flux–profile relationships. *Boundary-Layer Meteorology* **7**: 363–372.
- Eichler A, Schwikowski M, Gäggeler H, Furrer V, Synal H, Beer J, Saurer M, Funk M. 2000. Glaciochemical dating of an ice core from the upper Grenzgletscher (4200 m a.s.l.). *Journal of Glaciology* **46**(154): 507–515.
- Escher-Vetter H. 1985a. Energy balance calculations for the ablation period 1982 at Vernagtferner, Oetztal Alps. *Annals of Glaciology* **6**: 158–160.
- Escher-Vetter H. 1985b. Energy balance calculations from five years meteorological records at Vernagtferner/Oetztal Alps. *Zeitschrift für Gletscherkunde und Glazialgeologie* **21**: 397–402.
- Fierz C, Plüss C, Martin E. 1997. Modelling the snow cover in a complex alpine topography. *Annals of Glaciology* **25**: 312–316.
- Föhn P. 1973. Short-term snow melt and ablation derived from heat- and mass-balance measurements. *Journal of Glaciology* **12**(65): 275–289.
- Funk M. 1985. Räumliche Verteilung der Massenbilanz auf dem Rhonegletscher und ihre Beziehung zu Klimatelementen. Zürcher Geographische Schriften 24, ETH Zürich.
- Gäggeler H, von Gunten HR, Rössler E, Oeschger H, Schotterer U. 1983. ²¹⁰Pb-dating of cold alpine firn/ice cores from Colle Gnifetti, Switzerland. *Journal of Glaciology* **29**(101): 165–177.
- Haeberli W, Schotterer HU, Wagenbach D, Haeberli-Schwitzer H, Bortenschlager S. 1983. Accumulation characteristics on a cold, high-alpine firn saddle from a snow-pit study on Colle Gnifetti, Monte Rosa, Swiss Alps. *Journal of Glaciology* **29**(102): 260–271.
- Hock R. 1999. A distributed temperature-index ice- and snowmelt model including potential direct solar radiation. *Journal of Glaciology* **45**(149): 101–111.
- Hock R, Noetzi C. 1997. Areal melt and discharge modelling of Storglaciären, Sweden. *Annals of Glaciology* **24**: 211–217.
- Hoelzle M, Mittaz C, Etzelmüller B, Haeberli W. 2001. Surface energy fluxes and distribution models of permafrost in European mountain areas: an overview of current developments. *Permafrost and Periglacial Processes* **12**: 53–68.
- Högström U. 1988. Non-dimensional wind and temperature profiles in the atmospheric surface layer: a re-evaluation. *Boundary-Layer Meteorology* **42**: 55–78.
- Konzelmann T, Braithwaite RJ. 1995. Variations of ablation, albedo and energy balance at the margin of the Greenland ice sheet, Kronprins Christian Land, eastern north Greenland. *Journal of Glaciology* **41**(137): 490–502.
- Konzelmann T, Ohmura A. 1995. Radiative fluxes and their impact on the energy balance of the Greenland ice sheet. *Journal of Glaciology* **41**(139): 490–502.
- Kuhn M. 1987. Micro-meteorological conditions for snow melt. *Journal of Glaciology* **33**(113): 263–272.
- La Casinière A. 1974. Heat exchange over a melting snow surface. *Journal of Glaciology* **13**(67): 55–72.
- Lehning M, Bartlett P, Brown B, Russi T, Stöckli U, Zimmerli M. 1999. Snowpack model calculations for avalanche warning based upon a network of weather and snow stations. *Cold Regions Science and Technology* **30**(1–3): 145–157.
- Lowe P. 1976. An approximating polynomial for the computation of saturation vapor pressure. *Journal of Applied Meteorology* **16**: 100–103.
- Martin S. 1975. Wind regimes and heat exchange on Glacier de Saint-Sorlin. *Journal of Glaciology* **14**(70): 91–105.
- Morris E. 1989. Turbulent transfer over snow and ice. *Journal of Hydrology* **105**: 205–223.
- Oerlemans J. 1992. Climate sensitivity of glaciers in southern Norway: application of an energy-balance model to Nigardsbreen, Hellstugubreen and Alftobreen. *Journal of Glaciology* **38**(129): 223–232.
- Oerlemans J. 2000. Analysis of a 3 year meteorological record from the ablation zone of Morteratschgletscher, Switzerland: energy and mass balance. *Journal of Glaciology* **46**(155): 571–579.
- Ohmura A. 1984. Comparative energy balance study for Arctic tundra, sea surface, glaciers and boreal forests. *Geo Journal* **8**(3): 221–228.
- Ohmura A. 2001. Physical basis for the temperature-based melt-index method. *Journal of Applied Meteorology* **40**: 753–761.
- Ohmura A, Gilgen H. 1993. Re-evaluation of the global energy balance. *Geophysical Monographs of the American Geophysical Union* **75**: 93–110.
- Oke TR. 1987. *Boundary Layer Climates*, 2nd ed. Routledge.
- Paerson WSB. 1994. *The Physics of Glaciers*, 3rd ed. Pergamon: New York.

- Philipona R, Fröhlich C, Betz C. 1995. Characterization of pyrgeometers and the accuracy of atmospheric long-wave radiation measurements. *Journal of Applied Optics* **34**(9): 1598–1605.
- Plüss C. 1997. The energy balance over an Alpine snowcover. *Zürcher Geographische Schriften* 65, ETH Zürich.
- Rossi G, Johnston P, Maggi V. 2000a. ALPCLIM project: reconstruction of the monthly values of solar radiation incident over the Lys Glacier surface (Monte Rosa — Western Italian Alps). In *26th International Conference on Alpine Meteorology — Innsbruck 11th September 2000*. ICAM.
- Rossi G, Johnston P, Maggi V. 2000b. Project ALPCLIM: résultats de l'observation météorologique dans le site de Colle du Lys (4250 mètres). In *Réunion Annuelle Société Hydrotechnique de France, Section Glaciologie. Grenoble 1er Mars 2000*. Société Hydrotechnique de France.
- Stull R. 1988. *An Introduction to Boundary Layer Meteorology*. Kluwer Academic Publishers.
- Suter S. 2002. Cold firm and ice in the Monte Rosa and Mont Blanc areas: spatial occurrence, surface energy balance and climatic evidence. Mitteilung 172, Versuchsanstalt für Wasserbau, Hydrologie und Glaziologie der ETH Zürich.
- Sverdrup H. 1936. The eddy conductivity of the air over a smooth snowfield. *Geofysiske Publikasjoner* **11**: 1–69.
- Van de Waal R, Oerlemans J, van der Hage J. 1992. A study of ablation variations on the tongue of Hintereisferner, Austrian Alps. *Journal of Glaciology* **38**(130): 319–324.
- Wagner HP. 1979. Strahlungshaushaltsuntersuchungen an einem Ostalpengletscher während der Hauptablationsperiode. Teil I: Kurzwellige Strahlung. *Archiv für Meteorologie, Geophysik und Bioklimatologie* **27**: 297–324.
- Wagner HP. 1980. Strahlungshaushaltsuntersuchungen an einem Ostalpengletscher während der Hauptablationsperiode. Teil II: Langwellige Strahlung und Strahlungsbilanz. *Archiv für Meteorologie, Geophysik und Bioklimatologie* **28**: 41–62.
- Wilson W. 1941. An outline of the thermodynamics of snowmelt. *Transactions of the American Geophysical Union* **22**: 182–195.